Beta-delayed neutron emission studies of ^{24}O

S. Neupane,[1,2,*] N. Kitamura,[1,3] Z. Y. Xu,[1] R. Grzywacz,[1,4] J. Heideman,[1] T. T. King,[4] M. Madurga,[1] K. Siegl,[1] P. Wagenknecht,[1] A. Chester,[5] B. Hu,[4] A. Richard,[2] J. Okołowicz,[6,7] M. Płoszajczak,[7] and S. J. Novario[8]

[1]*Department of Physics and Astronomy, University of Tennessee, Knoxville, Tennessee 37996 USA*
[2]*Lawrence Livermore National Laboratory, Livermore, California 94551 USA*
[3]*Center for Nuclear Study, University of Tokyo, Wako, Saitama 351-0198, Japan*
[4]*Physics Division, Oak Ridge National Laboratory, Oak Ridge, Tennessee 37831 USA*
[5]*Facility for Rare Isotope Beams, Michigan State University, East Lansing, Michigan 48824 USA*
[6]*Institute of Nuclear Physics, Polish Academy of Sciences, Radzikowskiego 152, PL-31342 Kraków, Poland*
[7]*Grand Accélérateur National d'Ions Lourds (GANIL), CEA/DSM - CNRS/IN2P3, BP 55027, F-14076 Caen Cedex, France*
[8]*Los Alamos National Laboratory, Los Alamos, New Mexico 87545 USA*

(Dated: November 23, 2025)

The β-delayed neutron energy spectrum of ^{24}O was measured for the first time. New half-life and branching ratios are extracted. The β-γ and β-delayed neutron measurements provided the excitation energies and β decay strength distribution to both neutron-bound and unbound states in ^{24}F. The decay of "doubly-magic" ^{24}O is an excellent case to benchmark the quality of the state-of-the-art calculations of the strength distribution near the neutron drip line. The experimental results are compared with the shell model calculation using the standard, empirical USDB interaction, novel ab initio calculations such as those using the valence-space in-medium similarity renormalization group (VS-IMSRG) and coupled cluster and also the shell model embedded in the continuum.

Introduction— Large proton-neutron asymmetry plays a pivotal role in altering the nuclear structure of unstable nuclei compared with their stable counterparts. Therefore, one of the prime focuses of the next generation of radioactive ion beam facilities is to characterize the structural evolution of the short-lived isotopes moving away from stability. Recent experimental efforts have revealed new phenomena in those exotic nuclei, such as the disappearance of conventional magic numbers and the emergence of new magic numbers [1, 2]. Another example is the peculiar behavior of the limits of nuclear binding. The neutron drip line in carbon ($Z = 6$), nitrogen ($Z = 7$), and oxygen ($Z = 8$) is experimentally known to be at $N = 16$. However, it rapidly extends to $N = 22$ for fluorine ($Z = 9$), and this sudden jump is referred to as the oxygen drip-line anomaly [3, 4]. As such, neutron-rich oxygen and fluorine isotopes are expected to provide a critical benchmark to study the effects of the spin-isospin dependent interaction, three-body forces, and the coupling to the continuum, which, in turn, determine the location of the neutron drip line [5, 6]. While ^{24}O is known to be the last bound isotope of the $Z = 8$ isotopic chain [3], a wealth of recent measurements indicated a spherical $N = 16$ shell closure originating from the large spin-orbit splitting between the neutron $d_{3/2}$ and $d_{5/2}$ orbitals. Consequently, ^{24}O is established as a doubly-magic drip-line nucleus [7–10]. The recent observation of the ^{28}O resonance, which decays to ^{24}O via four neutron emissions, also emphasized the doubly-magic nature of ^{24}O [11].

The β decay of neutron-rich oxygen isotopes provides a means to probe the transition into fluorine. In particular, the decay of ^{24}O should be simple; to first order, the allowed Gamow-Teller (GT) transitions can be described by transforming either a $d_{5/2}$ neutron to a $d_{5/2}$ proton, or a $s_{1/2}$ neutron to a $s_{1/2}$ proton. As a result, 1^+ states in ^{24}F with relatively pure configurations are populated, owing to the selectivity of the GT transition. Hence, decay studies of ^{24}O are uniquely suited to test nuclear models that aim to describe the nuclear structure approaching the neutron drip line and beyond. Due to the large β-decay Q-value (Q_β) of 10.97(19) MeV [12], the β decay of ^{24}O populates both bound and unbound states in ^{24}F, the latter lying above its neutron separation energy of 3.81(10) MeV [12], thus allowing for the β-delayed neutron emission. Neutron spectroscopy provides unique access to the neutron unbound states in the daughter, which are otherwise difficult to study by other means.

The β decay of ^{24}O was first studied by Mueller et al. [13], and they reported a half-life of 61^{+31}_{-19} ms and a neutron branching ratio of 58(12) %. A similar measurement, performed by Reed et al. [14], reported a half-life of 65(5) ms, which agrees within the uncertainty given in the earlier measurement, but indicated a significantly lower neutron branching ratio of 18(6) %. Later, Penionzhkevich et al. [15] reported a similar half-life of 67(10) ms and a neutron branching ratio of 12(8) %. However, the most recent measurement performed by Caceres et al. [16] presented a slightly longer half-life of 80(5) ms and again a higher neutron branching ratio of 43(4) %.

The bound excited states at 521 and 1830 keV in ^{24}F were first identified by Reed et al. and this result was confirmed by Caceres et al. Both measurements assigned spins and parities of 2^+ and 1^+ to the 521 and 1830 keV states, respectively. Furthermore, Caceres et al. per-

* neupane1@llnl.gov

formed a complementary measurement using in-beam γ spectroscopy, and three new excited states in ^{24}F at 2384, 2739, and 3562 keV were proposed. However, states above the neutron threshold (S_n) have not yet been explored. By employing both γ and neutron spectroscopy, we extend our knowledge of ^{24}F above S_n, providing a deeper insight into the nuclear structure of this neutron-rich isotope next to ^{24}O.

Experiment— The experiment was performed at the National Superconducting Cyclotron Laboratory at Michigan State University. A primary beam of ^{48}Ca was accelerated to a kinetic energy of 140 MeV/nucleon using the Couple Cyclotron Facility [17] and directed onto an 846-mg/cm^2 thick beryllium target, producing a secondary cocktail beam by projectile fragmentation. The isotopes of interest were separated from all other reaction products and guided to the experimental area using the A1900 fragment separator [18]. The isotopes were identified on an event-by-event basis by measuring the time-of-flight between a plastic scintillator in the A1900 focal plane and a silicon PIN detector upstream of the experimental setup and the energy loss in the PIN detector.

The experimental setup, shown in Fig. 1, includes a scintillator array for neutrons and germanium clovers for γ rays. At the heart of the setup is an Yttrium Orthosilicate (YSO) scintillator-based detector [19], which was used for identifying ion implantation and their subsequent β decay events. The YSO implantation detector is 12 mm thick and has an active surface area of 48×48 mm^2, which was segmented into 24×24 pixels. Its backside was coupled to a position-sensitive multianode photomultiplier tube (MAPMT), H12700B-10 [20], via a 5-mm-thick acrylic light guide. The MAPMT has 8×8 anode and common dynode outputs. The dynode provides energy and timing measurements, while the anodes are used for the two-dimensional hit-position reconstruction. An Anger logic resistive network [21] was employed to reduce the number of anode channels down to four. Each of the dynode and the four anode signals were split and recorded with two different gain settings. A set of five signals (four anodes and one dynode) in the high-gain mode, i.e., with external amplification, was used for recording β events. The low-gain branch without amplification was dedicated to ion implantation events. By utilizing the timing and position information, β events can be correlated with their corresponding implants.

The Versatile Array of Neutron Detectors at Low Energy (VANDLE) [22, 23] was used for TOF measurements of β-delayed neutrons. A full array consisting of 48 plastic scintillator bars, resulting in a total neutron detection efficiency of 11% at 1 MeV, was placed at a distance of 105 cm measured between the center of the implantation detector and the front face of the bar. The high-gain dynode signal of the implantation detector provided the start timing of neutron TOF measurements. Three high-purity germanium clovers for γ-ray detection were installed on the other side of the setup. These detectors provided a total photopeak efficiency of 1.3% at 1 MeV.

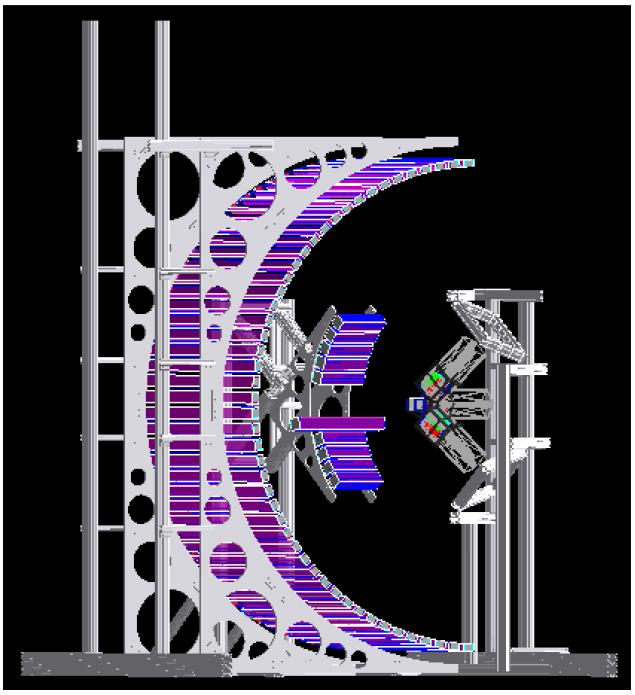

FIG. 1: Schematic view of the experimental setup with all detector systems and supporting materials. The experimental setup comprised 48 VANDLE bars for neutron measurements, three germanium clovers for γ-ray detection, and an YSO-based detector for identifying ion implantation and β-decay events. An array of ten newly-developed neutron detectors [24, 25] was also present but was not utilized in the present data analysis because of the low geometric efficiency.

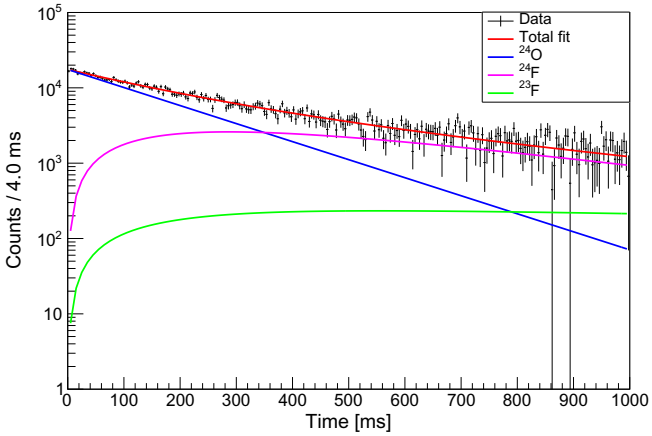

FIG. 2: Background-subtracted decay curve for ^{24}O obtained in the present measurement. The total fit, calculated using the Bateman equations, is shown in red. The individual components of ^{24}O and its daughters, i.e., ^{24}F and ^{23}F, are shown in blue, magenta, and green, respectively.

Analysis and Results—

Ion-β correlation was taken using the ^{24}O implantation and β-decay events measured in the YSO detector. In the present analysis, a correlation time window of ±1000 ms

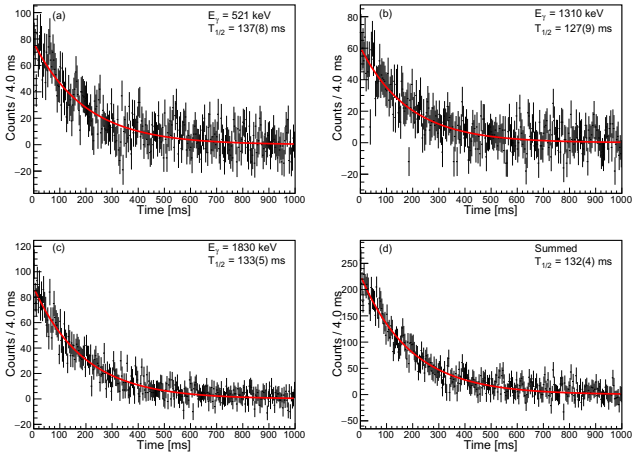

FIG. 3: Background-subtracted decay curve for ^{24}O obtained gated on individual γ transitions (a) - (c) and the sum of all gamma transitions (d) in ^{24}F.

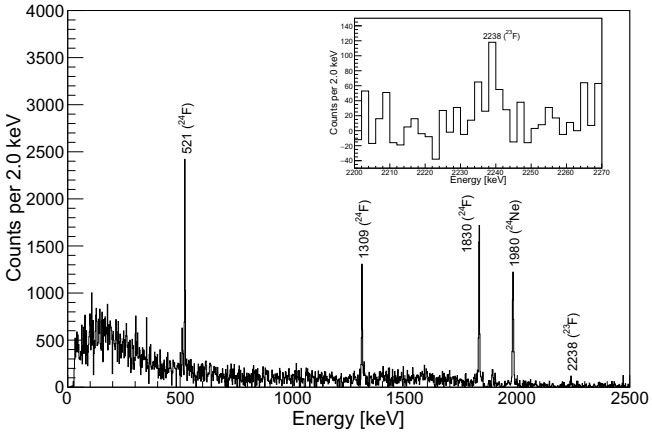

FIG. 4: Background-subtracted γ-ray spectrum following the decay of ^{24}O occurring within 500 ms after implantation. An add-back procedure was used. The background was estimated by gating on the negative correlation time of 500 ms on the decay curve. The inset shows the spectrum zoomed around 2238 keV γ ray.

TABLE I: Half-lives of various isotopes obtained in the present measurement compared with the literature values [26–29]. The error includes both statistical and systematic components. Except for ^{24}O, the present values show excellent agreement with the literature.

Isotope	This work (ms)	Literature (ms)
^{18}C	92(2)	90(2) [26]
^{22}N	23(1)	23(3) [27]
^{23}N	15.8(15)	14.1^{+12}_{-13} [28]
^{24}O	125(9)	72(5)[a]

[a] Weighted average of Refs. [13, 14, 16] as in Ref. [29]

TABLE II: Beta feeding intensities (I_β) and log ft values for the GT states in ^{24}F. These states are labeled by their excitation energies (E_x) measured from the ground state.

E_x (keV)	I_β (%)	log ft
1830(2)	62.2(118)	4.3(1)
5031(22)	10.4(21)	4.2(1)
5684(37)	11.4(21)	3.9(1)
6223(51)	7.2(17)	3.9(1)

was opened, and the events contained within the negative correlation time, i.e., before the implant, were used to model the background originating from random β signals associated with each implant. The decay curve after the background subtraction is shown in Fig. 2, together with the best fit to the data. The Bateman equations were employed to account for the decay of the daughters. From the fit, a half-life of 125(9) ms was obtained for the ^{24}O decay. The quoted error includes both statistical and systematic uncertainties, the latter arising from preset parameters in the fitting, namely, the half-lives of the daughters and the neutron branching ratio of the ^{24}O decay. The half-life obtained in this work is significantly longer than the literature values [13–16]. To validate the analysis procedure, half-lives of other nuclei were extracted from the same data set. As summarized in Table I, the half-lives of ^{18}C, ^{22}N, and ^{23}N from the present measurement were found to give excellent agreement with the literature values. Decay curves created by gating on γ transitions in ^{24}F provided another verification of the updated half-life of ^{24}O, as shown in Fig. 3.

The β-delayed γ-ray spectrum of ^{24}O, with add-back enabled, is shown in Fig. 4. A shorter ion-β correlation window of $\pm$500 ms was chosen for optimized spectral quality. The γ-ray peaks at 521, 1309, and 1830 keV, reported in the previous β-γ measurements [14, 16], were clearly identified in the present spectrum. These are attributed to two bound excited states in ^{24}F. From the γ-γ coincidence analysis, it was confirmed that the state at 1830 keV is predominantly populated in the β decay, and it deexcites by emitting a 1830 keV γ ray or via a cascade of 1309- and 521-keV γ rays. An intensity balance consideration placed the 1309-keV transition on top of the 521-keV γ ray. A log ft value of 4.3(1) obtained for the 1830 keV state suggests a GT transition, and therefore, a spin-parity assignment of 1^+ was given to this state. The present measurement also confirms the very weak direct population of the 512-keV state, and this is in line with the 2^+ assignment discussed in the previous works, as well as the ground-state spin-parity of 3^+, made based on comparisons with shell-model calculations (see Refs. [14, 16] for details).

Figure 5 presents the β-delayed neutron TOF spectrum obtained for the ^{24}O decay. Three well-separated neutron peaks, with energies ranging from 1.2 to 2.4 MeV, were observed in this spectrum. Since two-neutron emission is energetically prohibited (S_{2n} = 11.39(10) MeV [12]), one-neutron emission from ^{24}F is the sole contributor to the spectrum. The three major neutron lines likely correspond to transitions that feed the ^{23}F ground state, considering their intensities. We note that the 2238 keV

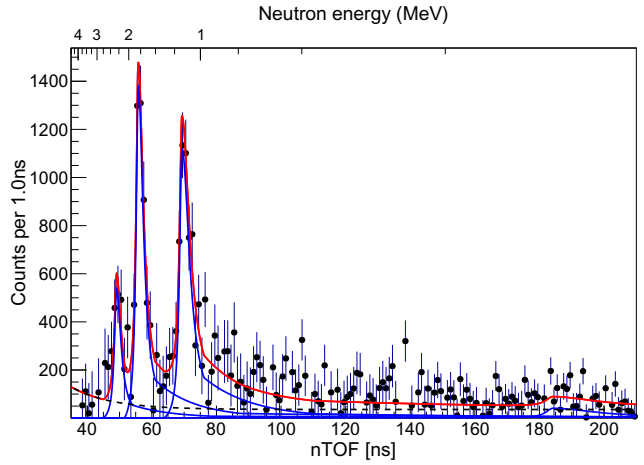

FIG. 5: Neutron singles TOF spectrum along with the analytical fitting function. The black points represent the measurement, and the total fitting function is shown in red. The contribution from individual peaks is shown in blue, and the dotted black line represents the background.

state in ^{23}F was observed with a weak feeding in the γ-ray spectrum (see the inset of Fig. 4). The neutron-γ cascade populating the 2238-keV state is possible from the 6632-keV state (see the level diagram in Fig. 6a), and this would produce a neutron with a kinetic energy of around 170 keV. Identifying such a neutron branch is challenging because of the limited statistics and the detection threshold in the present experiment. The neutron spectrum hints at a small peak at ∼185 ns; however, it awaits future experimental verification.

To determine the energies of the neutron peaks and their number of counts, the neutron TOF spectrum was fitted with a combination of template detector response functions and an exponential background. The response functions were generated by Geant4 [30, 31] simulations that use the exact geometry of the detector system, as can be seen in Fig. 1 and validated by the three well-established, prominent neutron lines of beta-delayed neutron emission from ^{17}N [32]. The fitting procedure is described in detail in Ref. [33]. The best fit is displayed in Fig. 5, and results obtained from the fit are summarized in Table II. The level energies in ^{24}F were reconstructed by summing the energy carried by neutron emission after correcting for recoil effects and the neutron separation energy. By normalizing the total number of neutrons feeding the excited and ground states of ^{23}F to the total number of β decays (N_β), a β-delayed neutron branching ratio of 28(5)% was obtained. Branching ratios for each state were obtained by normalizing the neutron intensities to N_β. $\log ft$ values were calculated using the half-life, excitation energies, and branching ratios from the present work, along with $Q_\beta = 10.97(19)$ MeV from Ref. [12]. For the three major neutron transitions, $\log ft$ values ranging from 3.9 to 4.2 were found. This favors GT transitions, leading to spin-parity assignments of 1^+ to these states.

Discussion— The GT transition strengths, B(GT), extending to neutron unbound states in ^{24}F, were deduced for the first time. The experimental level energies and strength distribution were then compared with predictions made by various nuclear models, namely, the phenomenological shell model, including that with continuum effects and state-of-the-art ab initio calculations. As a starting point of the discussion, we performed shell-model calculations with the USDB effective interaction [34]. This empirical shell-model interaction, constructed within the *sd*-shell model space, has been shown to give reliable predictions of nuclear properties in this mass region. To benchmark ab initio nuclear models, calculations were performed using two different approaches, the valence space in-medium similarity renormalization group (VS-IMSRG) [35, 36] and the coupled-cluster (CCSDT-1) [37] methods. In the IMSRG calculations, the Hamiltonian was derived using the 1.8/2.0 (EM) interaction [38] and diagonalized in the *sd*-shell model space. In calculating B(GT), effects arising from two-body currents are taken into account [39]. In order to study the roles played by the coupling to the continuum, level energies and B(GT) strengths were calculated using the shell model embedded in the continuum (SMEC) approach [40]. The results of these theoretical calculations are displayed in Fig. 6 together with the experimental values.

The USDB, VS-IMSRG, and CCSDT-1 calculations consistently reproduce the bound-state structure of ^{24}F. Guided by these results, the spins and parities of the ground (first-excited) states are highly likely 3^+ (2^+). The location of the first 1^+ state, as well as its GT strength, are in good agreement with the predictions by these models. However, discrepancies become more pronounced above the neutron threshold. As such, the unbound 1^+ states provide a critical testing ground for different theoretical models. The USDB calculations predict the location of the unbound states remarkably well, although the GT strengths to these states tend to be underestimated. The ab initio calculations, VS-IMSRG and CCSDT-1, show more concentrated strength distributions, which are in conflict with the experimental observation. The CCSDT-1 produces a state with a strong strength around 9 MeV, which was not seen in any other calculations. It is noted that USDB, IMSRG, and CCSDT-1 predicted a 1^+ state near the neutron separation energy with a small GT strength. The non-observation of this state in the experiment can be attributed to the small β feeding. A low detection efficiency for high-energy γ rays or the lack of sensitivity to low-energy neutrons would provide an additional explanation.

In addition to level energies and decay strengths, the SMEC calculations are capable of calculating the natural decay widths of the unbound states. With a continuum coupling strength V_0 of 150 MeV fm^3, the widths of the neutron-emitting states are predicted to be 10–40 keV. However, due to the limitations coming from

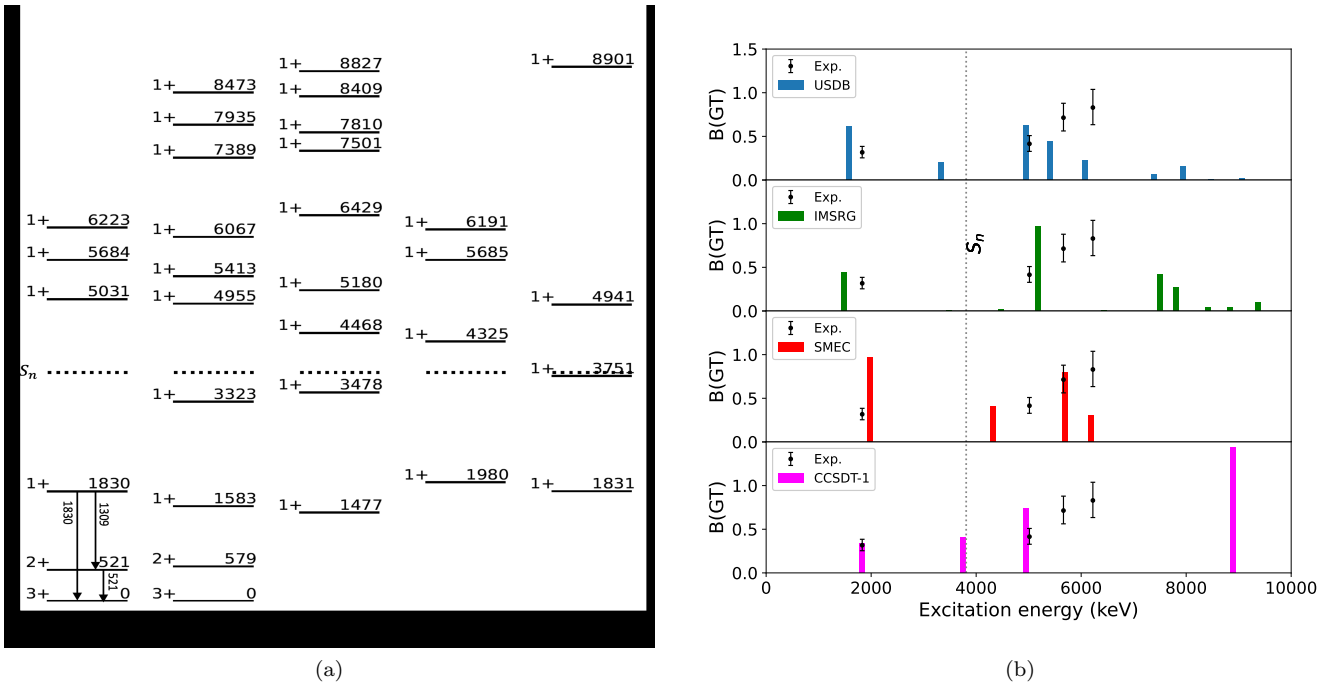

(a) (b)

FIG. 6: (a) Experimental energies and (b) GT transition strengths, B(GT), associated with the observed 1^+ states in ^{24}F, in comparison with various nuclear model calculations. Shell-model results using the empirical USDB interaction, and ab initio calculations using the valence space in-medium similarity renormalization group (VS-IMSRG) and the coupled-cluster model (CCSDT-1), as well as predictions from the shell model embedded in the continuum (SMEC) are shown.

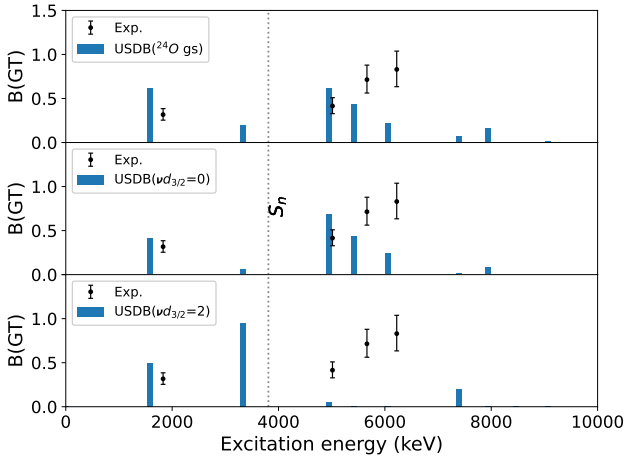

FIG. 7: The experimental decay strengths are compared with the calculations using USDB interaction in different scenarios: (top panel) considering ^{24}O ground state, (middle panel) neutron occupation in $d_{3/2}$ in ^{24}O forced to 0 and (bottom panel) neutron occupation in $d_{3/2}$ in ^{24}O forced to 2.

statistics and the detector resolution, it was not possible to extract the widths from the present measurement. Instead, an upper limit on the widths for the two prominent peaks was found to be 45 keV in 1σ. Future publications will highlight the determination of the decay widths of neutron-emitting states, which was made possible by an experiment performed at the Facility for Rare Isotope Beams (FRIB).

In order to investigate the roles played by neutron excitations involving the $d_{3/2}$ orbital, calculations with different shell-model truncation settings have been performed using the USDB interaction. Figure 7 displays the results of these calculations. The original USDB calculation, which has an average $\nu d_{3/2}$ occupation number of 0.125 in the ^{24}O ground state, is shown in the top panel. No significant changes were seen in B(GT) when the neutron occupation number in the $\nu d_{3/2}$ orbital is set to 0, as shown in the middle panel. However, forcing the neutron occupation number to 2 resulted in a sizable B(GT) reduction above S_n, as opposed to the experimental observation (see the bottom panel). This suggests that the $\nu d_{3/2}$ orbital remains at high single-particle energy, thus creating a spherical $N = 16$ shell closure in ^{24}O, as was indicated in the previous measurements.

Clearly, the experimental investigation of the ^{24}O decay provided a very robust test of the shell model and ab initio calculations. The inability of the calculations to reproduce the decay properties of this reasonably simple nucleus highlighted deficiencies of the nuclear models, especially for the nuclei far from stability where effects of three-nucleon forces and coupling to the continuum play

an important role.

Conclusion— We have reported the first β-delayed neutron spectroscopy of ^{24}O. Combining γ-ray spectroscopy, the half-life and neutron emission probability of the ^{24}O decay were significantly updated, and more complete β decay strengths extending to the neutron unbound states in ^{24}F were obtained. The new experimental data allowed for comparisons with various theoretical calculations. Shell model calculations using the standard USDB interaction, although not perfect, produced a fairly good overall agreement with the measured, suggesting that the transition from ^{24}O to ^{24}F can be described without invoking dramatic changes to the shell structure that go beyond the current empirical predictions. The present data has provided important tests of ab initio type calculations using the IMSRG and CC approaches. These calculations are found to well reproduce the structure of ^{24}F around its ground state. However, disagreements are more pronounced for the neutron unbound states. This implies that predicting the decay properties of the neutron-rich nucleus is not trivial and optimizations are still required. The determination of the natural widths of the neutron unbound states discovered in the present experiment will shed more light on the roles of the coupling to the continuum and can be used to benchmark state-of-the-art nuclear models.

ACKNOWLEDGMENTS

This research was partly sponsored by the National Nuclear Security Administration under the Stewardship Science Academic Alliances program through DOE Cooperative Agreements No. DE-NA0003899 and DE-NA0004068. This research was also sponsored by the Office of Nuclear Physics, U.S. Department of Energy, under contract DE-FG02-96ER40983 (UT) and DE-SC0020451 (MSU). This research was sponsored in part by the National Science Foundation under the contract NSF-MRI-1919735. This work was also supported by the National Nuclear Security Administration through the Nuclear Science and Security Consortium under Award No. DE-NA0003180 and the Stewardship Science Academic Alliances program through DOE Award No. DOE-DE-NA0003906.

[1] T. Otsuka, A. Gade, O. Sorlin, T. Suzuki, and Y. Utsuno, Rev. Mod. Phys. **92**, 015002 (2020).
[2] O. Sorlin and M.-G. Porquet, Progress in Particle and Nuclear Physics **61**, 602 (2008).
[3] Y. Kondo, T. Nakamura, R. Tanaka, R. Minakata, S. Ogoshi, N. Orr, N. Achouri, T. Aumann, H. Baba, F. Delaunay, *et al.*, Physical Review Letters **116**, 102503 (2016).
[4] T. L. Tang, T. Uesaka, S. Kawase, D. Beaumel, M. Dozono, T. Fujii, N. Fukuda, T. Fukunaga, A. Galindo-Uribarri, S. H. Hwang, N. Inabe, D. Kameda, T. Kawahara, W. Kim, K. Kisamori, M. Kobayashi, T. Kubo, Y. Kubota, K. Kusaka, C. S. Lee, Y. Maeda, H. Matsubara, S. Michimasa, H. Miya, T. Noro, A. Obertelli, K. Ogata, S. Ota, E. Padilla-Rodal, S. Sakaguchi, H. Sakai, M. Sasano, S. Shimoura, S. S. Stepanyan, H. Suzuki, M. Takaki, H. Takeda, H. Tokieda, T. Wakasa, T. Wakui, K. Yako, Y. Yanagisawa, J. Yasuda, R. Yokoyama, K. Yoshida, K. Yoshida, and J. Zenihiro, Phys. Rev. Lett. **124**, 212502 (2020).
[5] T. Otsuka, T. Suzuki, J. D. Holt, A. Schwenk, and Y. Akaishi, Physical review letters **105**, 032501 (2010).
[6] G. Hagen, M. Hjorth-Jensen, G. Jansen, R. Machleidt, and T. Papenbrock, Physical Review Letters **108**, 242501 (2012).
[7] A. Ozawa, T. Kobayashi, T. Suzuki, K. Yoshida, and I. Tanihata, Physical review letters **84**, 5493 (2000).
[8] R. Kanungo, C. Nociforo, A. Prochazka, T. Aumann, D. Boutin, D. Cortina-Gil, B. Davids, M. Diakaki, F. Farinon, H. Geissel, *et al.*, Physical review letters **102**, 152501 (2009).
[9] C. Hoffman, T. Baumann, D. Bazin, J. Brown, G. Christian, D. Denby, P. DeYoung, J. Finck, N. Frank, J. Hinnefeld, S. Mosby, W. Peters, W. Rogers, A. Schiller, A. Spyrou, M. Scott, S. Tabor, M. Thoennessen, and P. Voss, Physics Letters B **672**, 17 (2009).
[10] K. Tshoo, Y. Satou, H. Bhang, S. Choi, T. Nakamura, Y. Kondo, S. Deguchi, Y. Kawada, N. Kobayashi, Y. Nakayama, *et al.*, Physical review letters **109**, 022501 (2012).
[11] Y. Kondo, N. Achouri, H. A. Falou, L. Atar, T. Aumann, H. Baba, K. Boretzky, C. Caesar, D. Calvet, H. Chae, *et al.*, Nature **620**, 965 (2023).
[12] M. Wang, W. Huang, F. Kondev, G. Audi, and S. Naimi, Chinese Physics C **45**, 030003 (2021).
[13] A. Mueller, D. Guillemaud-Mueller, J. Jacmart, E. Kashy, F. Pougheon, A. Richard, A. Staudt, H. Klapdor-Kleingrothaus, M. Lewitowicz, R. Anne, *et al.*, Nuclear Physics A **513**, 1 (1990).
[14] A. T. Reed, O. Tarasov, R. D. Page, D. Guillemaud-Mueller, Y. E. Penionzhkevich, R. G. Allatt, J. C. Angélique, R. Anne, C. Borcea, V. Burjan, W. N. Catford, Z. Dlouhý, C. Donzaud, S. Grévy, M. Lewitowicz, S. M. Lukyanov, F. M. Marqués, G. Martinez, A. C. Mueller, P. J. Nolan, J. Novák, N. A. Orr, F. Pougheon, P. H. Regan, M. G. Saint-Laurent, T. Siiskonen, E. Sokol, O. Sorlin, J. Suhonen, W. Trinder, and S. M. Vincent, Phys. Rev. C **60**, 024311 (1999).
[15] Y. E. Penionzhkevich, Physics of Atomic Nuclei **64**, 1121 (2001).
[16] L. Cáceres, A. Lepailleur, O. Sorlin, M. Stanoiu, D. Sohler, Z. Dombradi, S. Bogner, B. Brown, H. Hergert, J. Holt, *et al.*, Physical Review C **92**, 014327 (2015).
[17] A. Stolz, T. Baumann, T. Ginter, D. Morrissey, M. Portillo, B. Sherrill, M. Steiner, and J. Stetson, Nuclear Instruments and Methods in Physics Research Section B: Beam Interactions with Materials and Atoms **241**, 858 (2005).

[18] D. Morrissey, B. Sherrill, M. Steiner, A. Stolz, and I. Wiedenhoever, Nuclear Instruments and Methods in Physics Research Section B: Beam Interactions with Materials and Atoms **204**, 90 (2003), 14th International Conference on Electromagnetic Isotope Separators and Techniques Related to their Applications.

[19] R. Yokoyama, M. Singh, R. Grzywacz, A. Keeler, T. King, J. Agramunt, N. Brewer, S. Go, J. Heideman, J. Liu, S. Nishimura, P. Parkhurst, V. Phong, M. Rajabali, B. Rasco, K. Rykaczewski, D. Stracener, J. Tain, A. Tolosa-Delgado, K. Vaigneur, and M. Wolińska-Cichocka, Nuclear Instruments and Methods in Physics Research Section A: Accelerators, Spectrometers, Detectors and Associated Equipment **937**, 93 (2019).

[20] Hamamatsu Photonics K. K., `https://www.hamamatsu.com/jp/en/index.html`.

[21] Vertilon Corporation, Westford, MA, `https://vertilon.com/`.

[22] W. Peters, S. Ilyushkin, M. Madurga, C. Matei, S. Paulauskas, R. Grzywacz, D. Bardayan, C. Brune, J. Allen, J. Allen, *et al.*, Nuclear Instruments and Methods in Physics Research Section A: Accelerators, Spectrometers, Detectors and Associated Equipment **836**, 122 (2016).

[23] S. Paulauskas, M. Madurga, R. Grzywacz, D. Miller, S. Padgett, and H. Tan, Nuclear Instruments and Methods in Physics Research Section A: Accelerators, Spectrometers, Detectors and Associated Equipment **737**, 22 (2014).

[24] J. Heideman, D. Pérez-Loureiro, R. Grzywacz, C. Thornsberry, J. Chan, L. Heilbronn, S. Neupane, K. Schmitt, M. Rajabali, A. Engelhardt, *et al.*, Nuclear Instruments and Methods in Physics Research Section A: Accelerators, Spectrometers, Detectors and Associated Equipment **946**, 162528 (2019).

[25] S. Neupane, J. Heideman, R. Grzywacz, M. Cooper, J. Hooker, K. L. Jones, T. T. King, N. Kitamura, M. Madurga, K. Siegl, C. R. Thornsberry, P. Wagenknecht, Z. Y. Xu, L. H. Heilbronn, M. M. Rajabali, A. Chester, A. Richard, Y. Alberty-Jones, J. Derkin, T. N. Massey, D. Soltesz, N. T. Brewer, B. C. Rasco, K. P. Rykaczewski, M. Wolinska-Cichocka, J. Clark, D. Santiago-Gonzales, and G. Savard, Phys. Rev. C **106**, 044320 (2022).

[26] J. Kelley and C. G. Sheu, ENSDF (2017).

[27] M. S. Basunia, Nuclear Data Sheets **127**, 69 (2015).

[28] M. Shamsuzzoha Basunia and A. Chakraborty, Nuclear Data Sheets **171**, 1 (2021).

[29] M. S. Basunia and A. Chakraborty, Nuclear Data Sheets **186**, 3 (2022).

[30] S. Agostinelli, J. Allison, K. Amako, J. Apostolakis, H. Araujo, P. Arce, M. Asai, D. Axen, S. Banerjee, G. Barrand, F. Behner, L. Bellagamba, J. Boudreau, L. Broglia, A. Brunengo, H. Burkhardt, and S. C. et al., Nuclear Instruments and Methods in Physics Research Section A: Accelerators, Spectrometers, Detectors and Associated Equipment **506**, 250 (2003).

[31] J. Allison, K. Amako, J. Apostolakis, P. Arce, M. Asai, T. Aso, E. Bagli, A. Bagulya, S. Banerjee, G. Barrand, B. Beck, A. Bogdanov, D. Brandt, J. Brown, H. Burkhardt, P. Canal, D. Cano-Ott, and S. C. et al., Nuclear Instruments and Methods in Physics Research Section A: Accelerators, Spectrometers, Detectors and Associated Equipment **835**, 186 (2016).

[32] H. Ohm, W. Rudolph, and K.-L. Kratz, Nuclear Physics A **274**, 45 (1976).

[33] Z. Y. Xu, M. Madurga, R. Grzywacz, T. T. King, A. Algora, A. N. Andreyev, J. Benito, T. Berry, M. J. G. Borge, C. Costache, H. De Witte, A. Fijalkowska, L. M. Fraile, H. O. U. Fynbo, A. Gottardo, C. Halverson, L. J. Harkness-Brennan, J. Heideman, M. Huyse, A. Illana, L. Janiak, D. S. Judson, A. Korgul, T. Kurtukian-Nieto, I. Lazarus, R. Lică, R. Lozeva, N. Marginean, R. Marginean, C. Mazzocchi, C. Mihai, R. E. Mihai, A. I. Morales, R. D. Page, J. Pakarinen, M. Piersa-Siłkowska, Z. Podolyák, P. Sarriguren, M. Singh, C. Sotty, M. Stepaniuk, O. Tengblad, A. Turturica, P. Van Duppen, V. Vedia, S. Viñals, N. Warr, R. Yokoyama, and C. X. Yuan, Phys. Rev. C **108**, 014314 (2023).

[34] B. A. Brown and W. A. Richter, Phys. Rev. C **74**, 034315 (2006).

[35] K. Tsukiyama, S. Bogner, and A. Schwenk, Physical review letters **106**, 222502 (2011).

[36] H. Hergert, S. Bogner, T. Morris, A. Schwenk, and K. Tsukiyama, Physics reports **621**, 165 (2016).

[37] G. Hagen, T. Papenbrock, D. J. Dean, A. Schwenk, A. Nogga, M. Włoch, and P. Piecuch, Phys. Rev. C **76**, 034302 (2007).

[38] K. Hebeler, S. K. Bogner, R. J. Furnstahl, A. Nogga, and A. Schwenk, Phys. Rev. C **83**, 031301 (2011).

[39] P. Gysbers, G. Hagen, J. D. Holt, G. R. Jansen, T. D. Morris, P. Navrátil, T. Papenbrock, S. Quaglioni, A. Schwenk, S. R. Stroberg, and K. A. Wendt, Nature Physics **15**, 428 (2019), arXiv:1903.00047 [nucl-th].

[40] J. Okołowicz, M. Płoszajczak, and I. Rotter, Physics Reports **374**, 271 (2003).

[41] A. Gade, C. K. Gelbke, and T. Glasmacher, Nuclear Physics News **24**, 28 (2014).

[42] C. S. Sumithrarachchi, D. J. Morrissey, A. D. Davies, D. A. Davies, M. Facina, E. Kwan, P. F. Mantica, M. Portillo, Y. Shimbara, J. Stoker, and R. R. Weerasiri, Phys. Rev. C **81**, 014302 (2010).

[43] Y. Utsuno, T. Otsuka, T. Mizusaki, and M. Honma, Phys. Rev. C **64**, 011301 (2001).

[44] M. Thoennessen, Reports on Progress in Physics **67**, 1187 (2004).

[45] B. Jonson, Physics Reports **389**, 1 (2004).

[46] B. A. Brown and W. Richter, Physical Review C **74**, 034315 (2006).

[47] B. A. Brown and W. A. Richter, Phys. Rev. C **74**, 034315 (2006).